Tuning the Dielectric Response of Water in Nanoconfinement through Surface Wettability

Ermioni Papadopoulou ,[†] Julija Zavadlav,*,[‡] Rudolf Podgornik,[¶,‖] Matej Praprotnik,[§,‖] and Petros Koumoutsakos[†]

[†]*Computational Science & Engineering Laboratory, ETH-Zurich, Clausiusstrasse 33, CH-8092 Zurich, Switzerland*
[‡]*Professorship of Multiscale Modeling of Fluid Materials, TUM School of Engineering and Design, Technical University of Munich, Germany*
[¶]*School of Physical Sciences and Kavli Institute for Theoretical Sciences, University of Chinese Academy of Sciences, Beijing, 100049, China & CAS Key Laboratory of Soft Matter Physics, Institute of Physics, Chinese Academy of Sciences, Beijing, 100190, China*
[§]*Laboratory for Molecular Modeling, National Institute of Chemistry, Hajdrihova 19, SI-1001 Ljubljana, Slovenia*
[‖]*Department of Physics, Faculty of Mathematics and Physics, University of Ljubljana, Jadranska 19, SI-1000 Ljubljana, Slovenia*

E-mail: julija.zavadlav@tum.de

Density Computation and Additional Results

The total average water density in channels (Table S1) is computed as $\rho = \frac{m_{H_2O}}{V_{H_2O}}$, where m_{H_2O} is the total mass of the water and $V_{H_2O} = l_x \, l_y \, h_{\text{eff}}$ is the total volume occupied by the water. Since the system is periodic, l_x, l_y correspond to the channel length and width, whereas h_{eff} is calculated for each trajectory as the available height for water molecules in the respective channel.

Table S1: Total density (with standard deviation) of confined water for varying heights of confinement h and wettabilities given by ϵ_{CO} or θ. The unconfined bulk density at ambient conditions is 1.01 ± 0.07 g/cm^3.

h [nm]	ρ [g/cm^3]
0.5	1.57 ± 0.07
0.8	1.32 ± 0.07
1.4	1.09 ± 0.09
2.2	1.03 ± 0.11
3.0	1.04 ± 0.09
3.5	1.02 ± 0.12
7.0	1.03 ± 0.12
10	1.03 ± 0.12
20	1.03 ± 0.11
30	1.02 ± 0.11

ϵ_{CO} [kcal/mol]	θ [°]	ρ [g/cm^3]
0.16369	7	1.1 ± 0.09
0.11369	52	1.06 ± 0.09
0.09369	80	1.03 ± 0.11
0.07369	110	1.01 ± 0.09
0.02369	157	0.95 ± 0.08

The density distributions (main text) are computed by splitting the corresponding channel height in bins of 0.05 nm and calculating the average and standard deviation of local density in each bin as $\rho_{bin} = \frac{m_{H_2O,bin}}{V_{H_2O,bin}}$, where $m_{H_2O,bin}$ is the local water mass and $V_{H_2O,bin}$ is the volume of each bin.

Dielectric Response Computation and Additional Results

The static dielectric constant of a liquid can be computed from the MD trajectories thought various routes. The standard way to calculate the dielectric constant of a bulk liquid is *via* fluctuations of the total dipole moment and the Clausius-Mosotti relation.[1–3] Since we simulate periodic systems, with the long-range electrostatics being calculated as an infinite continuum reaction field $\varepsilon_{RF} = \infty$, through the Particle-Mesh Ewald summation, the relation corresponds to

$$\varepsilon^{(M)} = 1 + \frac{< \mathbf{M}^2 > - < \mathbf{M} >^2}{3\varepsilon_0 V k_B T}, \tag{S1}$$

where V is the total volume of the system, T temperature of the system, ε_0 the vacuum permittivity, and k_B the Boltzmann constant. The total dipole moment is $\mathbf{M} = \sum \boldsymbol{\mu}$, where $\boldsymbol{\mu}$ is the molecular dipole moment. To compute the normal component of the dielectric

constant $\varepsilon_\perp^{(M)}$ we use

$$\varepsilon_\perp^{(M)} = 1 + \frac{<M_\perp^2> - <M_\perp>^2}{\varepsilon_0 V k_B T}, \tag{S2}$$

where $M_\perp = \sum \mu_\perp$. Similarly, the perpendicular component is computed using $\mathbf{M}_\parallel = \sum \mu_\parallel$ and

$$\varepsilon_\parallel^{(M)} = 1 + \frac{<M_\parallel^2> - <M_\parallel>^2}{2\varepsilon_0 V k_B T}. \tag{S3}$$

The computed averages and standard deviation of the total, the normal and the parallel component of the dielectric constant of bulk water (using a system of 6845 water molecules in the isothermal-isochoric ensemble at 298 K), computed with the aforementioned method are respectively $\varepsilon^{(M)} = 80.253 \pm 0.65$, $\varepsilon_\perp^{(M)} = 81.554 \pm 0.94$ and $\varepsilon_\parallel^{(M)} = 80.403 \pm 0.4$ and match results of previous studies.[4]

The anomalous dielectric constant of liquid water in strong confinement has been studied for many years, and stems from the interfacially induced polarization of water, altering its dielectric response.[5,6] Furthermore, for planar confinements, the dielectric profile is known to be anisotropic and therefore the calculation of the dielectric constant profile under confinement is fully characterized by the parallel and normal components of the dielectric constant with respect to the surface of confinement.[7–9]

The calculation of the normal component of dielectric constant from the MD simulation trajectories in this study follows the method of Balleneger *et al.*[7] From the instantaneous MD trajectory, after folding the coordinates on periodic boundaries, we determine the profile of the charge density ρ_q along the channel height (Figure S1a,c) defined as

$$\rho_q(z) = \frac{1}{l_x l_y \Delta z} \sum_i e_i \delta(z - z_i), \tag{S4}$$

where the summation runs over all the water. A bin width of 0.01 nm was used. The laterally averaged normal polarization density $m_\perp$ is calculated along the channel height

$$m_\perp(z) = -\int_0^z \rho_q(z')\mathrm{d}z', \tag{S5}$$

which, integrated over the entire channel height, results in the total polarization

$$M_\perp = l_x l_y \int_0^h m_\perp(z)\mathrm{d}z, \tag{S6}$$

where $l_x l_y$ is the lateral channel area. The normal component of polarization correlation function is then calculated as

$$c_\perp(z) = \langle m_\perp(z) M_\perp \rangle - \langle m_\perp(z) \rangle \langle M_\perp \rangle. \tag{S7}$$

The inverse normal dielectric profile along the channel height is computed as

$$\varepsilon_\perp^{-1}(z) = 1 - \frac{c_\perp(z)}{\varepsilon_0 k_B T}. \tag{S8}$$
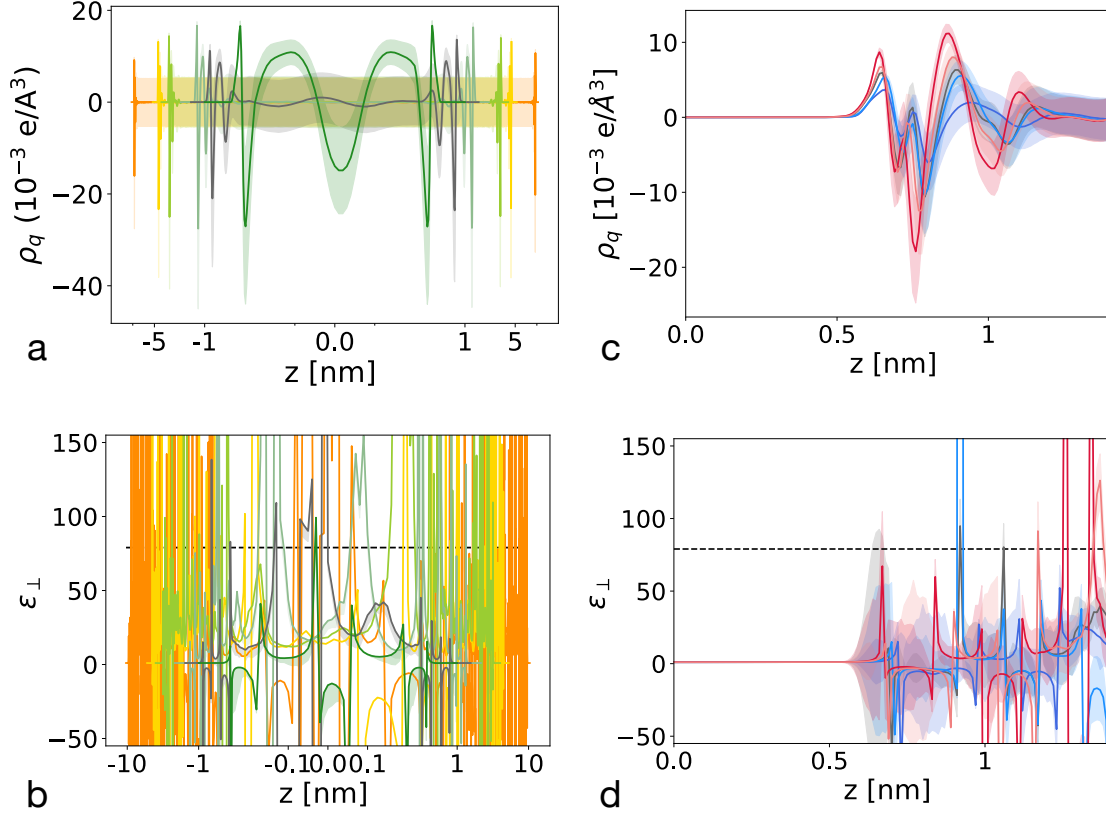
Figure S1: Spatial distribution of the charge density ρ_q (a,c) and the perpendicular dielectric response (b,d) along the the channel height. The x-axis for (a,b) is in symmetric logarithmic scale with z = 0 denoting the middle of the channel, while for (c,d) z = 0 denotes the position of the wall. (a,b) The green, grey, sea green, light green, gold and orange curves correspond to the channel heights of $h = 1.4, 2.2, 3.5, 7, 10, 20$ nm, respectively. (c,d) The red, light red, grey, light blue and blue curves correspond to contact angles of $7, 52, 80, 110, 157°$. The shaded region around the solid lines represent the standard deviation, whereas the black dashed lines correspond to the bulk value. In all graphs, the grey curve refers to the same case of h and θ.

The distribution $\varepsilon_\perp^{-1}(z)$, which is shown in the manuscript can be inverted to give $\varepsilon_\perp(z)$ shown in Figure S1b,d, using bin width of 0.01 nm. To obtain the overall or effective dielectric constant $\varepsilon_\perp$ in the channel domain (Table S2) we use

$$\int_0^h \varepsilon_\perp^{-1}(z)\mathrm{d}z = h_{eff}\left[\frac{1}{\varepsilon_\perp} - 1\right] - h\,, \tag{S9}$$

where h is the height of the water confinement, whereas h_{eff} is the effective height of the channel. The difference $\delta h = h - h_{eff} = 3.19$ nm corresponds to the free space water can expand to, with respect to the interaction parameter σ_{CO}, therefore does not vary with the channel height or surface wettability, $i.e.$, we only vary ϵ_{CO} while σ_{CO} is kept constant. The calculation of $\varepsilon_{\perp,I}$ is performed in the same manner, $i.e.$, replacing h in Eq. S9 with $h_I + \frac{\delta h}{2}$, where the width of the interface region h_I is determined through the tetrahedral

distributions to equal $h_I = 0.9$ nm.

The parallel component of the dielectric constant profile is again calculated following the methodology of Ballenegger *et al.*[7] In this case, the total parallel polarization is defined in the same way as for the normal component, as the integral of the lateral average polarization density

$$M_\parallel(z) = l_x l_y \int_0^h m_\parallel(z) \mathrm{d}z. \tag{S10}$$

We compute two components, respectively in the x and the y directions. For each direction x or y, the average polarization density $m_\parallel(z)$ is computed as the average of the surface charge $P_0(x/y, z)$. The surface charge in each direction $P_0(x/y, z)$ is computed by making cuts in the respective direction x or y and adding the charges of the atoms below the cut. This is different from the calculation of the local charge density ρ_q, as the boundary of a bin might split the atoms of a water molecule, leaving some charges in every bin. Since we are dealing with vectors of the parallel polarization in two directions, the parallel polarization correlation function is now calculated as

$$c_\parallel(z) = \langle m_\parallel(z) M_\parallel \rangle - \langle m_\parallel(z) \rangle \langle M_\parallel \rangle, \tag{S11}$$

where $\langle m_\parallel(z) M_\parallel \rangle$ is the ensemble average of the quantity $m_x(z) M_x + m_y(z) M_y$ and $\langle m_\parallel(z) \rangle \langle M_\parallel \rangle$ is computed as the vector product $\langle m_x(z) \rangle \langle M_x \rangle + \langle m_y(z) \rangle \langle M_y \rangle$. The parallel dielectric profile is then obtained with

$$\varepsilon_\parallel(z) = 1 + \frac{c_\parallel(z)}{\varepsilon_0 k_B T}. \tag{S12}$$

To obtain the overall or effective dielectric constant $\varepsilon_\parallel$ in the channel domain (Table S2 and in the manuscript), we use

$$\varepsilon_\parallel = 1 + \frac{\left[\int_0^h \varepsilon_\parallel(z) \mathrm{d}z \right] - h}{h_{eff}}, \tag{S13}$$

At this point, we note that the behavior of the $\varepsilon_\parallel$ changes, according to the definition. In the manuscript and for the rest of this study, we use the effective $\varepsilon_\parallel$ definition. However, if instead of computing the effective $\varepsilon_\parallel$, we simply average the raw data within each region, we obtain lower absolute values of $\varepsilon_\parallel$ (Fig. S2). We also notice that upon decreasing the channel height, $\varepsilon_\parallel$ is first reduced to values below the bulk value and then increases above the bulk value for the smallest two channel heights. Using the definition of the average $\varepsilon_\parallel$, upon modifying the wettability from hydrophilic to hydrophobic ($\theta \uparrow$), the parallel component is decreased by 30%, as opposed to the effective $\varepsilon_\parallel$ variation, which was reported equal to 31% in the manuscript.

For the capacitance model, we fit the interfacial dielectric components dependency on the wettability of the channel surface. The following relations are extracted:

$$\varepsilon_{\perp,I}[\theta(\epsilon_{CO})] = -45.93 \epsilon_{CO}^2 - 3.44 \epsilon_{CO} + 4.79 \tag{S14}$$

and

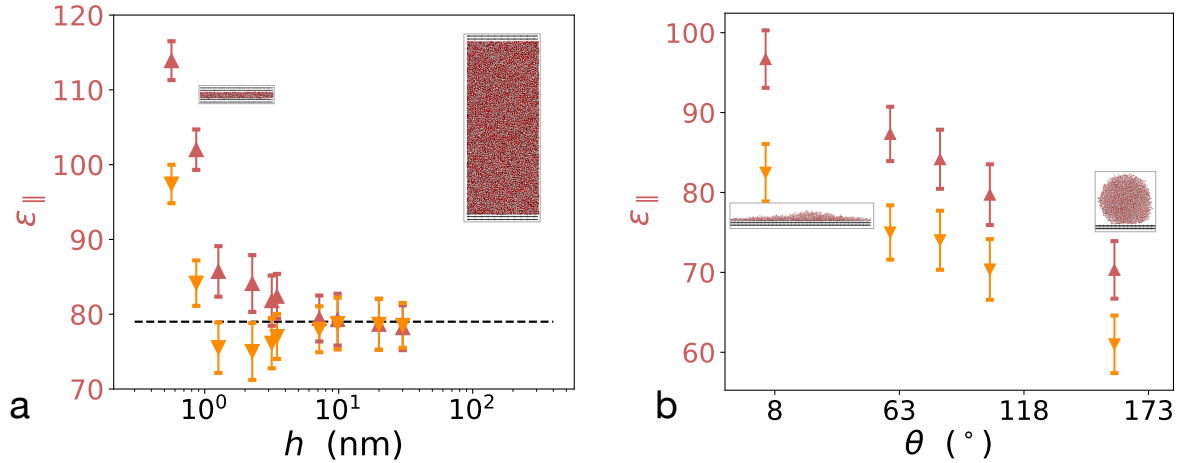$$\varepsilon_{\parallel,I}[\theta(\epsilon_{CO})] = -162.03 \epsilon_{CO}^2 + 232.55 \epsilon_{CO} + 66.87. \tag{S15}$$

Figure S2: Parallel dielectric response of water in confinement for various (a) heights and (b) surface wettabilities. The effective parallel $\varepsilon_\parallel$ (red markers) and average parallel $\varepsilon_\parallel$ (orange markers) components of the dielectric constant of water are calculated along the whole height of the confinement. The error bars denote the standard deviation. (a) Bulk value of the dielectric constant of water is denoted with the dashed black line.

Table S2: Average values and standard deviations of the perpendicular ($\varepsilon_\perp$) and parallel ($\varepsilon_\parallel$) dielectric constant of confined water for varying heights h of the channel wettabilities ϵ_{CO}. Results are reported for different regions: interfacial (denoted with subscript "I"), bulk (region excluding the interfacial region, denoted with subscript "B") and the overall region (without the subscript).

h [nm]	$\varepsilon_{\perp,I}$	$\varepsilon_{\perp,B}$	$\varepsilon_\perp$	$\varepsilon_{\parallel,I}$	$\varepsilon_\parallel$
0.5	-	-	1.81±1.25	-	113.9±2.6
0.8	-	-	2.49±1.55	-	102.0±2.7
1.4	-	-	3.06±2.21	-	85.7±3.4
2.2	3.91±2.44	54.9±5.5	4.18±2.4	87.54±3.7	84.1±3.8
3.0	4.15±2.34	64.6±5.9	4.67±2.26	93.93±3.3	81.82±3.4
3.5	3.99±1.92	65.7±5.9	5.45±2.10	97.3±3	82.4±3.1
7.0	4.08±1.68	75.8±5.6	11.53±2.59	99.4±3.7	79.43±3.5
10	4.25±1.84	75.9±5.5	15.79±3.53	98.3±3.5	79.28±3.4
20	4.08±1.9	76.5±3.64	29.58±3.93	88.57±3.9	78.65±3.4
30	4.24±2.44	78.5±3.06	36.2±3.12	87.94±2.8	78.2±3

ϵ_{CO} [kcal/mol]	θ [°]	$\varepsilon_{\perp,I}$	$\varepsilon_\perp$	$\varepsilon_{\parallel,I}$	$\varepsilon_\parallel$
0.16369	7	3.02±2.59	3.38±2.2	100.7±3.5	96.69±3.6
0.11369	52	3.72±2.37	3.90±2.2	90.73±3.5	87.33±3.5
0.09369	80	4.15±2.26	4.18±2.4	87.54±3.7	84.15±3.7
0.07369	110	4.29±2.25	4.31±2.1	83.29±3.3	79.72±3.8
0.02369	157	4.68±2.54	4.90±2.2	72.21±3.2	70.3±3.6

We note that in the manuscript all plots that refer to variation of the surface wettability are given with respect to the contact angle θ of a water droplet on a graphene sheet, setting the strength of the Lennard-Jones interaction between carbon and oxygen ϵ_{CO}. To retrieve the relation between contact angle θ to the corresponding interaction strength ϵ_{CO}, we performed five simulations, letting a droplet of SPC/Fw water equilibrate on a graphene flat surface, varying the interaction strength $\epsilon_{CO} = 0.16369, 0.11369, 0.09369, 0.07369, 0.02369$ kcal/mol. The computation of the contact angle of water droplets on planar surfaces follows the method introduced in Werder *et al.*[10] The measured contact angles at the end of the equilibration were respectively: $\theta = 7, 52, 80, 110, 157°$. We retrieve a linear relation between the interaction strength ϵ_{CO} and the contact angle θ, *i.e.*, $\theta = 184 - 1100\,\epsilon_{CO}$ (Figure S3).
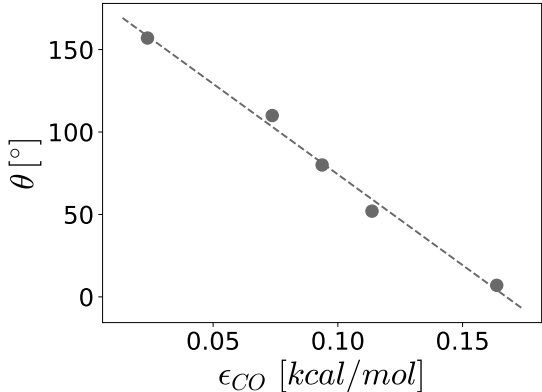

Figure S3: Contact angle of SPC/Fw water droplet equilibrated on a flat graphene-like surface as a function of interaction strength ϵ_{CO}.

Order Parameters Definitions and Additional Results

The first two order parameters $\eta^{(1),(2)}$ are defined as

$$\eta^{(1)} = \langle \cos \phi \rangle \tag{S16}$$

and

$$\eta^{(2)} = \frac{1}{2} \langle 3 \cos^2 \phi - 1 \rangle, \tag{S17}$$

where ϕ is the angle between the dipole moment of water and the vector normal to the channel wall. If all molecules are exactly aligned with the vector normal to the interface $\theta = 0$ for all molecules, which means that $\eta^{(1,2)} = 1$. When all molecules lie in the plane perpendicular to the normal, but randomly oriented in that plane, the angles is $\theta = \pi/2$ for all molecules so that $\eta^{(1)} = 0$ and $\eta^{(2)} = -1/2$. In the isotropic phase, $\eta^{(1,2)} = 0$.[11] The third order parameter, $\eta^{(3)}$ corresponds to the quadrupole moment of water in the direction of the
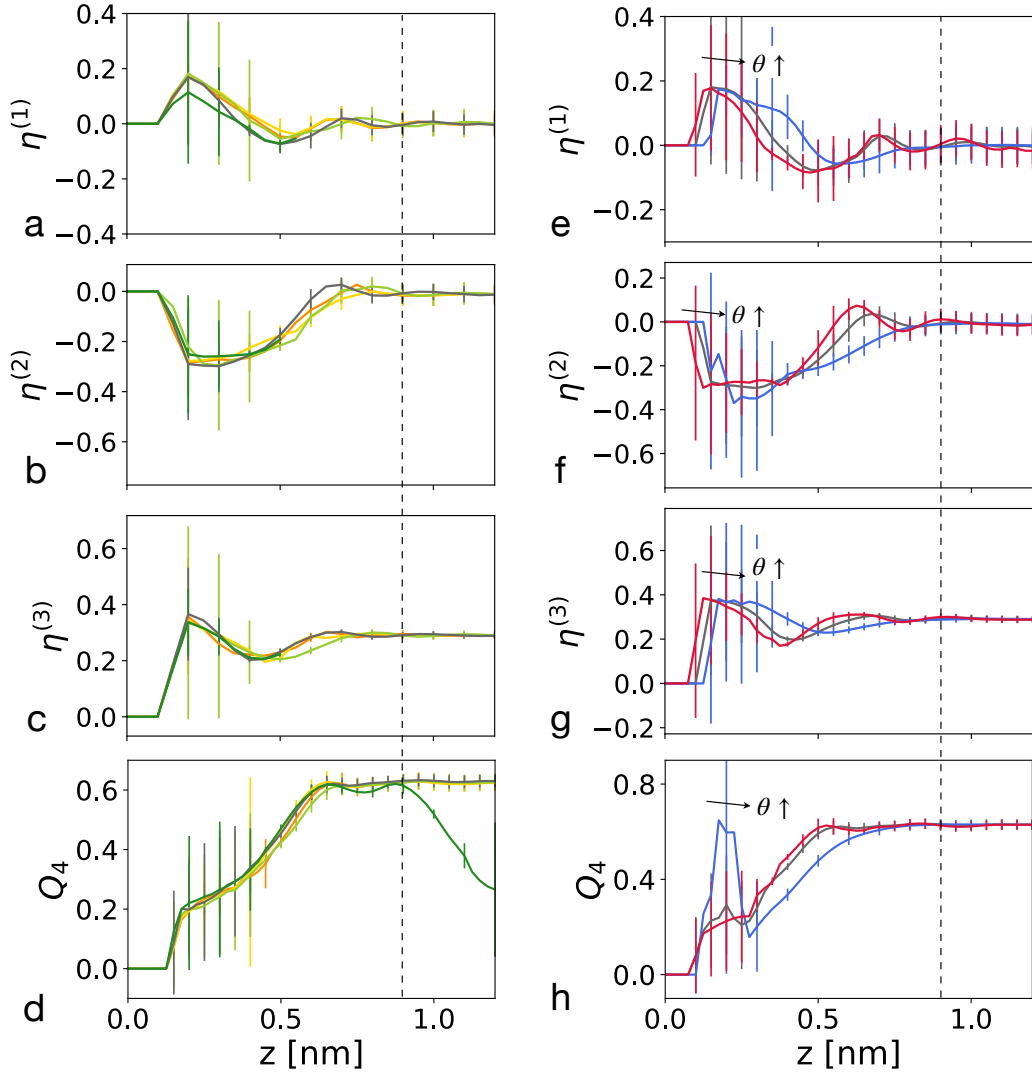
Figure S4: Order parameters $\eta^{(1,2,3)}$ and Q_4 for varying confinement heights (a-d) and surface wettabilities (e-h) as a function of distance from the channel wall. (a-d) The green, grey, sea green, light green, gold and orange curves correspond to channels with wettability contact angle $\theta = 80°$ and heights $h = 1.4, 2.2, 3.5, 7, 10, 20$ nm, respectively. (e-h) The red, grey and blue curves correspond to a channel of $h = 2.2$ nm and $\theta = 7, 80, 157°$, respectively. In all graphs, the grey curve refers to the same case of h and θ. The black dashed line denotes the extent of the interface region $h_I = 0.9$ nm. The error bars represent the standard deviations.

channel height and is calculated with

$$\eta^{(3)} = \langle \sum_i q_i r_i^2 \rangle, \tag{S18}$$

where the summation runs over the hydrogen atoms with charge q_i that are at distance r_i from the oxygen atom in the z-direction (direction of channel height). The value of the quadrupole moment away from the boundary is $\approx 3.0 \cdot 10^{-3}$ e_0/nm^2, which corresponds to

the value of $\eta^{(3)}$ of bulk water.[12]

The fourth order parameter Q_4 corresponds to the tetrahedrality of water is defined as

$$Q_4(z) = \left\langle 1 - \frac{3}{8} \sum_{j=1}^{3} \sum_{k=j+1}^{4} \left(\cos\theta_{ijk} + \frac{1}{3} \right)^2 \right\rangle, \tag{S19}$$

where the summation runs over pairs of the closest neighboring molecules j, k of each water molecule i and θ_{ijk} is the the angle formed by the lines joining the oxygen atom of the water molecule under consideration i and its nearest neighbor oxygen atoms j and k. A tetrahedral order parameter $Q_4 = 1$ denotes a regular tetrahedron, whereas $Q_4 = 0$ denotes a random distribution. The average bulk, unconfined value for water is $Q_4 \approx 0.6$.[13]

For all order parameter definitions, the brackets $\langle \dots \rangle$ denote averaging over the course of the simulation trajectory. The spatial distribution of the order parameters (Figure S4) is obtained by spatially splitting the domain and averaging in bins of 0.025 nm. The results are averaged over both interface regions, $i.e.$, at both ends of the channel.

The distributions of $\eta_B^{(1)}$ and $Q_{4,B}$ in the bulk region, $i.e.$, the region excluding the interface layer (Figure S5), are obtained by splitting the range of possible values into 100 bins.
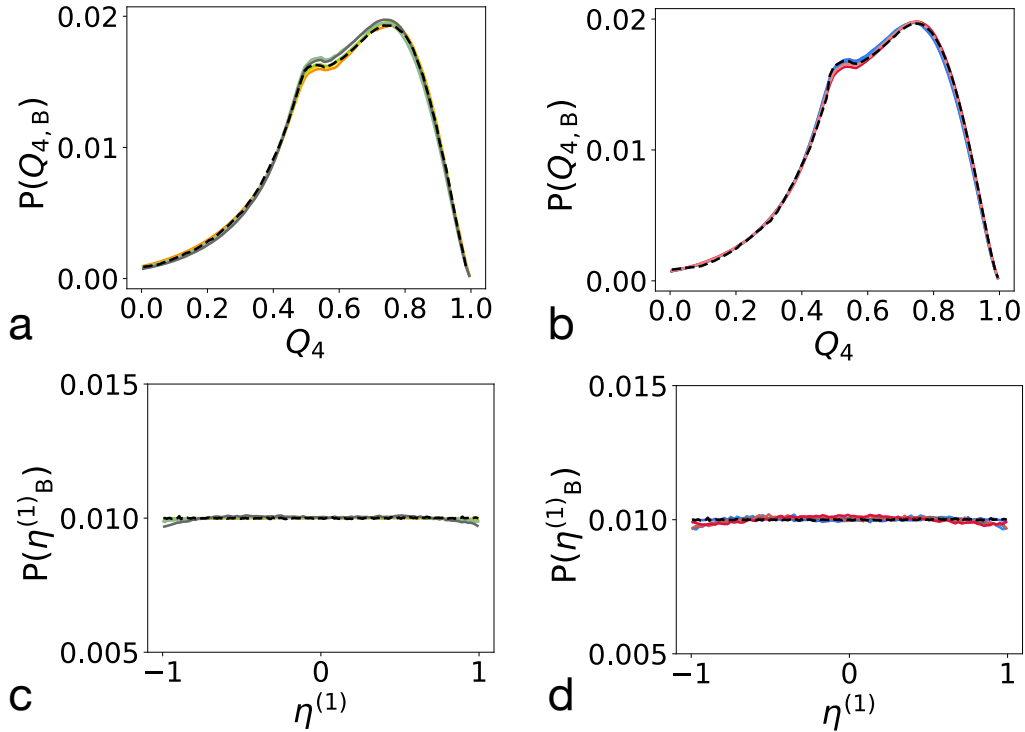

Figure S5: The distribution of $Q_{4,B}$ (a,b) and $\eta_B^{(1)}$ in the bulk region for varying channel heights (a,c) and wettabilities (b,d). The green, grey, sea green, light green, gold and orange curves correspond to channels with wettability contact angle $\theta = 80°$ and heights $h = 1.4, 2.2, 3.5, 7, 10, 20$ nm, respectively. The red, light red, grey, light blue and blue curves correspond to a surface channel of $h = 2.2$ nm and $\theta = 7, 52, 80, 110, 157°$ respectively. In all graphs, the grey curve refers to the same case of h and θ. The black dashed curves in all subfigures correspond to the distribution of the bulk, unconfined water.

We perform a sensitivity study, regarding the size of the interface layer for varying surface wettability. For channel height $h = 2.2$ nm, we vary the surface wettability to correspond to a contact angle $\theta = 7, 80, 157°$ (Figure S6) and we probe the tetrahedrality distribution in thin regions of size 0.1 nm, centered at increasing distances from the channel wall. We find that, although the Q_4 distribution at the layers in proximity to the wall surface are greatly affected by the surface wettability, the size of the interface layer is not affected by the surface wettability, as above $h = 0.9$ nm the Q_4 distribution collapses to the bulk $P(Q_4)$ of water, regardless of the surface wettability.
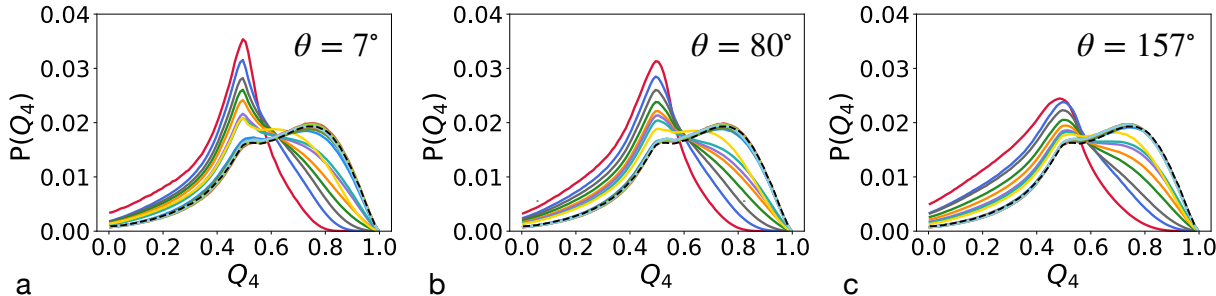

Figure S6: The distribution of Q_4 probed in slabs of 0.1 nm thickness at increased distance (from 0.2 to 1 nm) from the channel wall. The profiles are shown for channel height $h = 2.2$ nm and for varying wettability from hydrophilic, $\theta = 7°$ (a), to neutral, $\theta = 80°$ (b) and hydrophobic, $\theta = 157°$ (c). The black dashed curves in all subfigures correspond to the Q_4 distribution of the bulk, unconfined water.

MD parameters tests

Interaction Cutoff

We test how MD parameters affect the results of this study, with the set of simulations of bulk, unconfined water. We vary the cutoff distance for the interaction between oxygens of water molecules between 8 to 12 Å and we find that a variation of the cutoff by 10% the calculated overall density and the dielectric constant are modified by less than 2%. Furthermore, no significant variation of the distribution of the dipole orientation and tetrahedrality are retrieved for varying cutoff values (Figure S7).

Dielectric constant, bin size

We perform a sensitivity analysis, showing that the computation of the profile of the out-of-plane dielectric component is robust to the choice of the bin size dz. Upon varying the bin size $dz = [0.1, 0.25, 0.5]$ nm, we find that the profile of the normal dielectric component does not change with the choice of the size of the bins along the height of the channel (Fig S8).
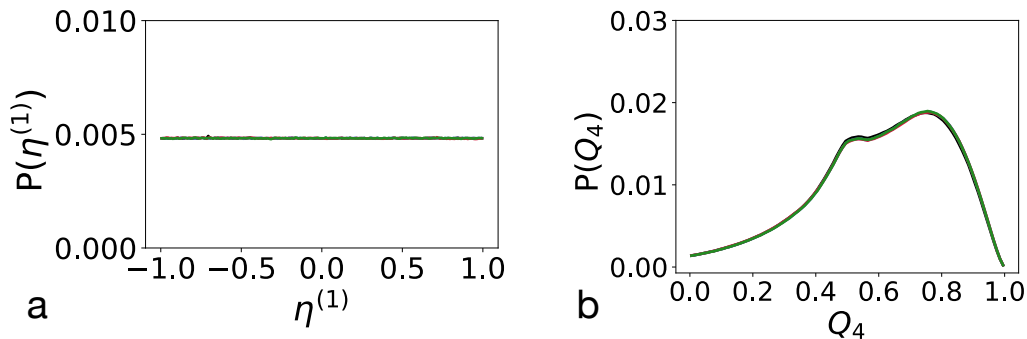
Figure S7: The distribution of $\eta^{(1)}$ (a) and Q_4 (b) of bulk, unconfined water for varying cutoff values for oxygen-oxygen interactions. The colored curves correspond to varying cutoff distances: red corresponds to 8 Å, black to cutoff 9 Å, blue to cutoff 10 Å, green to 12 Å.
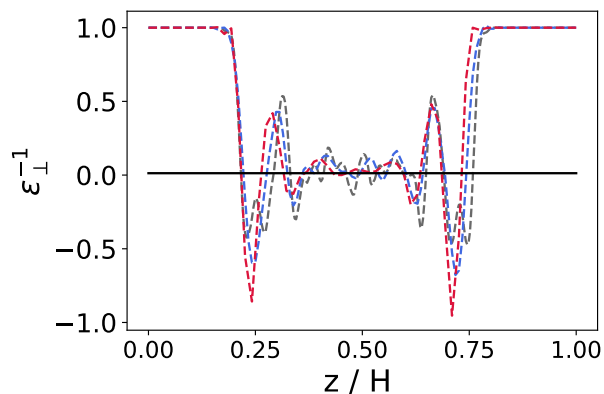

Figure S8: The profile of $\varepsilon_\perp$ along the channel height for $h = 2.2$ nm, for varying bin size dz. corresponds to 8 Å, black to cutoff 9 Å, blue to cutoff 10 Å, green to 12 Å.

References

(1) Neumann, M. Dipole Moment Fluctuation Formulas in Computer Simulations of Polar Systems. *Mol. Phys.* **1983**, *50*, 841–858.

(2) Kirkwood, J. G. The Dielectric Polarization of Polar Liquids. *J. Chem. Phys.* **1939**, *7*, 911–919.

(3) Raabe, G.; Sadus, R. J. Molecular Dynamics Simulation of the Dielectric Constant of Water: The Effect of Bond Flexibility. *J. Chem. Phys.* **2011**, *134*.

(4) Wu, Y.; Tepper, H. L.; Voth, G. A. Flexible Simple Point-Charge Water Model with Improved Liquid-State Properties. *J. Chem. Phys.* **2006**, *124*, 024503.

(5) Bonthuis, D. J.; Gekle, S.; Netz, R. R. Dielectric Profile of Interfacial Water and Its Effect on Double-Layer Capacitance. *Phys. Rev. Lett.* **2011**, *107*, 166102.

(6) De Luca, S.; Kannam, S. K.; Todd, B. D.; Frascoli, F.; Hansen, J. S.; Daivis, P. J. Effects of Confinement on the Dielectric Response of Water Extends up to Mesoscale Dimensions. *Langmuir* **2016**, *32*, 4765–4773.

(7) Ballenegger, V.; Hansen, J. P. Dielectric Permittivity Profiles of Confined Polar Fluids. *J. Chem. Phys.* **2005**, *122*, 114711.

(8) Ghoufi, A.; Szymczyk, A.; Renou, R.; Ding, M. Calculation of Local Dielectric Permittivity of Confined Liquids from Spatial Dipolar Correlations. *EPL* **2012**, *99*, 37008.

(9) Schlaich, A.; Knapp, E. W.; Netz, R. R. Water Dielectric Effects in Planar Confinement. *Phys. Rev. Lett.* **2016**, *117*, 1–5.

(10) Werder, T.; Walther, J. H.; Jaffe, R. L.; Halicioglu, T.; Koumoutsakos, P. On the Water-Carbon Interaction for Use in Molecular Dynamics Simulations of Graphite and Carbon Nanotubes. *J. Phys. Chem. B.* **2003**, *107*, 1345–1352.

(11) Mottram, N. J.; Newton, C. J. P. Introduction to Q-Tensor Theory. **2014**, arXiv:1409.3542v2 [cond-mat.soft]. `https://arxiv.org/pdf/1409.3542.pdf` (accessed 11 15, 2021).

(12) Coudert, F. X.; Cailliez, F.; Vuilleumier, R.; Fuchs, A. H.; Boutin, A. Water Nanodroplets Confined in Zeolite Pores. *Faraday Discuss.* **2009**, *141*, 377–398.

(13) Duboué-Dijon, E.; Laage, D. Characterization of the Local Structure in Liquid Water by Various Order Parameters. *J. Phys. Chem. B.* **2015**, *119*, 8406–8418.